

Supplementary Materials: Tying together multiscale calculations for charge transport in P3HT: structural descriptors, morphology, and tie-chains

Evan D. Miller ¹, Matthew L. Jones ¹ and Eric Jankowski ^{1,*}

1. ZINDO and DFT Comparison

In this section, we compare the ZINDO calculation of electronic properties used in this investigation, to a more rigorous DFT method to determine the accuracy of semi-empirical frontier molecular orbital energy calculations for P3HT. We use three representative P3HT chromophore pairs selected from an equilibrated, ordered test morphology, visualizations of which are depicted in [Figure S1](#). The DFT calculations were performed using the B3LYP functional [1] and the 6311++g** basis set [2].

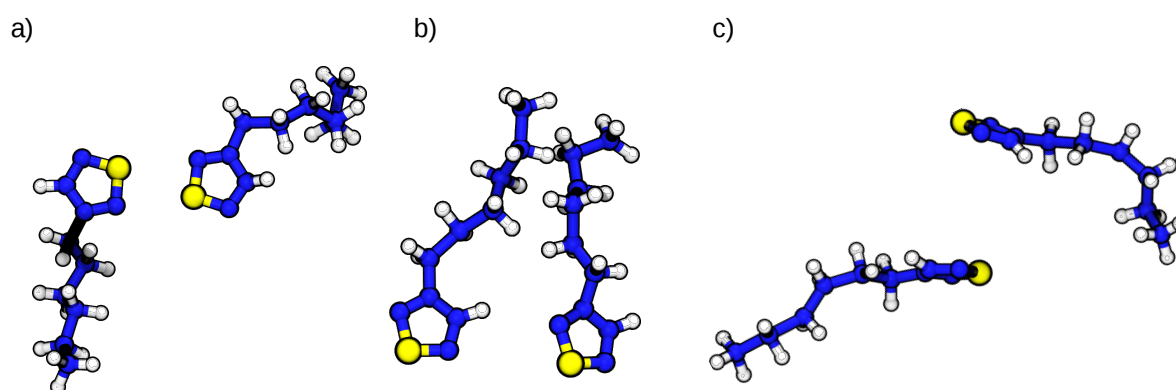


Figure S1. The three representative chromophore pairs used to investigate the accuracy of the ZINDO/S semiempirical method. a) 0469-3714, b) 0841-1237, c) 2032-2900. Terminating hydrogens were added for the QCCs based on position in the thiophene ring.

Table S1. A comparison of the HOMO splitting and calculated transfer integrals for three representative P3HT chromophore pairs

HOMO Splitting	DFT (eV)	ZINDO/S (eV)
0469-3714	0.196	0.095
0841-1237	0.199	0.058
2032-2900	0.086	0.008

The calculated electronic properties of the chromophore pairs are shown in [Table S1](#). ZINDO appears to consistently underpredict the HOMO splitting, which would lead to lower transfer integrals and slower transport than expected from more rigorous DFT methods. However, the ZINDO calculations provide good agreement with the DFT results to within ~ 100 meV, which is already the rough cutoff for DFT accuracy. Furthermore, changes in transfer integral of factors of 2-3 are not expected to significantly affect the charge transport properties given that morphological changes can result in orders of magnitude differences. ZINDO calculations can be performed within 5-10 seconds for a chromophore pair, compared to several minutes to half an hour in the case of more rigorous DFT calculations (depending on the DFT level desired). As such, the computational throughput is significantly improved at the cost of the smaller reduction in accuracy - a critically important point given that each morphology can contain upwards of 40,000 chromophore pairs to be considered.

In summary, the vastly improved computational efficiency at the cost of a small reduction in accuracy of ZINDO/S justifies our use of the semi-empirical calculations for our charge transport properties instead of more rigorous DFT methodologies.

2. Developing ψ' to Explicitly Consider Transfer Integrals

One possible short-coming in our modified order parameter ψ' is that it is an indirect predictor of the electronic transfer integral $J_{i,j}$ between two chromophores. The hopping rate between two chromophores is strongly dependent on the electronic transfer integral $J_{i,j}$ (see Equation 2 of the main

26 text) and the energy level difference $\Delta E_{i,j}$ of the two chromophores. Additionally, $\Delta E_{i,j}$ is also partially
 27 encoded into $J_{i,j}$, in which chromophores with incompatible energy levels (for instance, a large $\Delta E_{i,j}$)
 28 will also reduce $J_{i,j}$ (see Equation 1 of the main text). As such, the transfer integral seems like a good
 29 “one-size-fits-all” parameter to describe clustering.

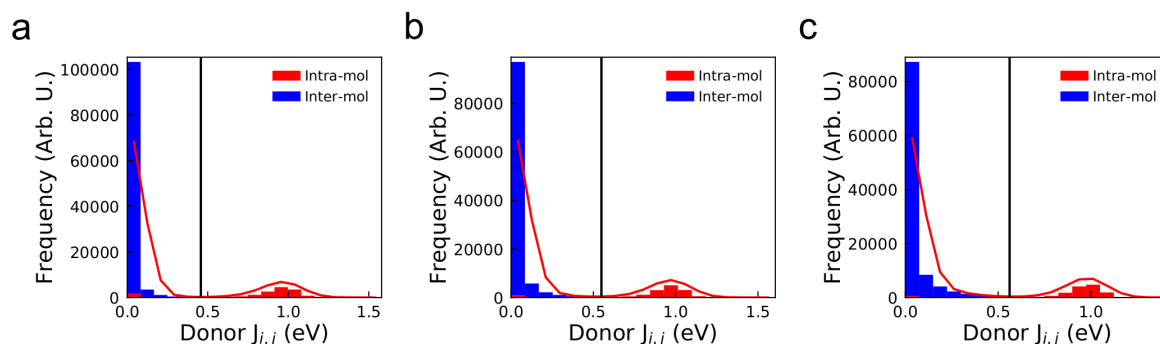


Figure S2. Distributions of chromophore Voronoi neighbor transfer integrals for the representative 1,000 molecule a) amorphous, b) semi-crystalline, and c) crystalline morphologies. The red line shows the Gaussian filtered distribution shape that was used to determine the cluster cut-off criterion. The black vertical line shows the value of the cut-off criterion, which was automatically determined to be at the minimum for each system - $J_{i,j} > 0.562, 0.549,$ and 0.457 eV for the crystalline, semi-crystalline, and amorphous morphologies respectively.

30 The transfer integral distributions for each representative system are shown in [Figure S2](#). In all
 31 three cases, the distribution has a large spike at very low transfer integrals and a bump at high TI
 32 corresponding to pairs within the same P3HT chain. Initially, we set the transfer integral cut-off to
 33 the location of the minimum for each morphology, such that only connections with transfer integrals
 34 greater than the cut-off are added to the same cluster. It is convenient to set cut-offs to maxima and
 35 minima as these can be determined automatically, rather than being calibrated manually for each
 36 separate system. For the crystalline, semi-crystalline, and amorphous morphologies, the cut-offs were
 37 set to $J_{i,j} > 0.562, 0.549,$ and 0.457 eV respectively.

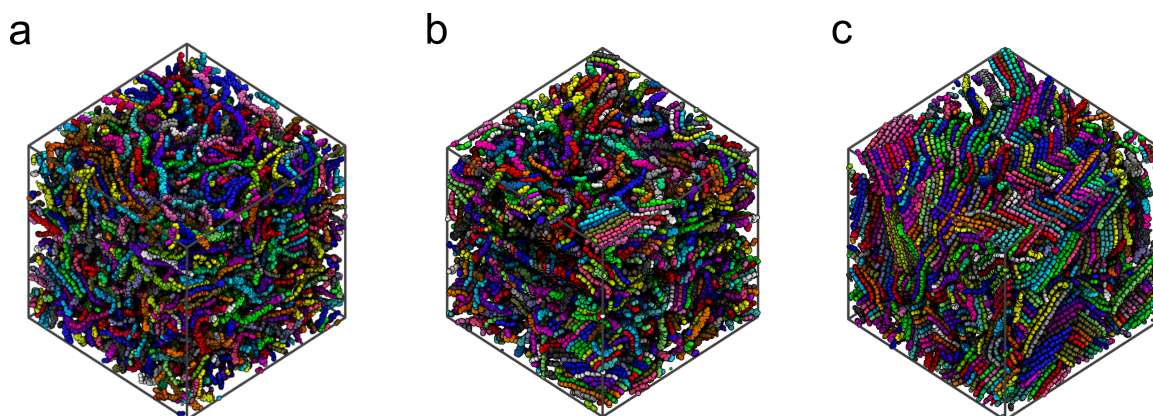


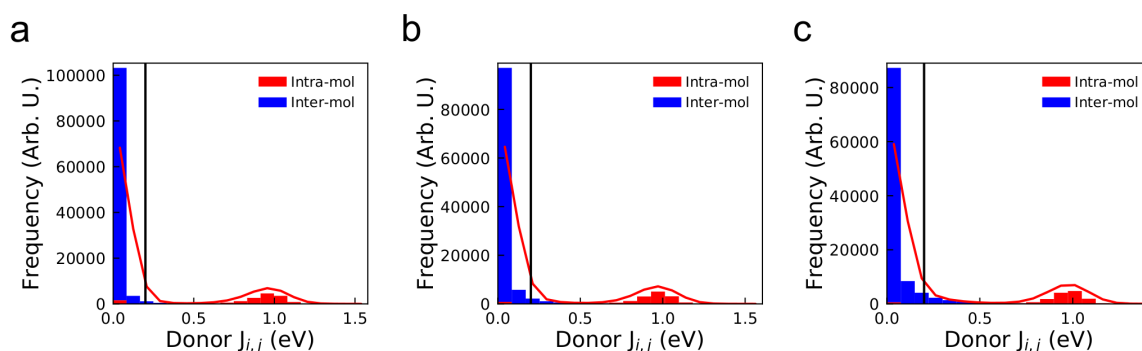
Figure S3. Visualizations of the clusters in the a) amorphous, b) semi-crystalline, and c) crystalline systems with size > 6 monomer units. Clusters were determined based on an automatically-defined transfer integral cut-off for each system based on the distributions in [Figure S2](#).

38 The resultant cluster visualization in [Figure S3](#) suggests that these cut-off values are too large -
 39 in all morphologies, hops with $J_{i,j} > \sim 0.5$ eV are generally only intra-molecular hops (red region in
 40 [Figure S2](#)). This leads to nearly every chain in the system being considered an individual cluster, with
 41 few occurrences of clusters forming between multiple chains. There is no significant difference in the

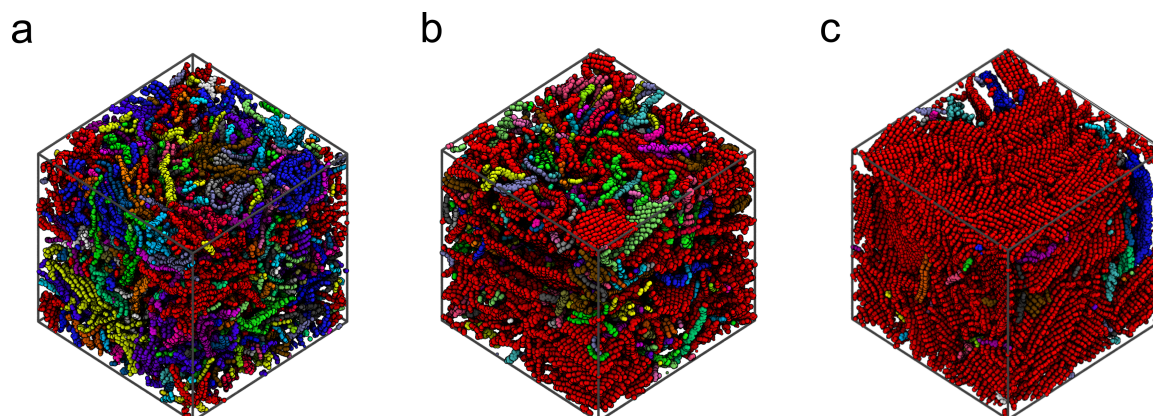
Table S2. Table of cluster statistics for the three systems, given the automatically-determined transfer integral cut-off criteria.

Property	Amorphous	Semi-Crystalline	Crystalline
Mobility (cm^2/Vs)	1.02×10^{-1}	1.63×10^{-2}	1.16×10^{-1}
$J_{i,j}$ cut-off (eV)	0.457	0.549	0.562
Total clusters (Arb. U.)	1067	1065	972
Large (> 6) clusters (Arb. U.)	964	941	873
Largest cluster size (Arb. U.)	60	60	90

42 cluster distribution throughout the morphology between the three systems, suggesting that a different
 43 transfer integral cut-off should be used.

**Figure S4.** Distributions of chromophore Voronoi neighbor transfer integrals for the representative 1,000 molecule a) amorphous, b) semi-crystalline, and c) crystalline morphologies. The red line shows the Gaussian filtered distribution shape that was used to determine the cluster cut-off criterion. The black vertical line shows the value of the cut-off criterion, $J_{i,j} > 0.2$ eV.

44 We can, for instance, reduce the cut-off to something smaller in order to include higher $J_{i,j}$
 45 inter-molecular hops. This however, has the short-coming in that such a selection will likely be
 46 arbitrarily chosen, not rather than an automatically identified minimum. Regardless, reducing the $J_{i,j}$
 47 cut-off to 0.2 eV (Figure S4) provides significantly improved results as now a non-negligible proportion
 48 of inter-molecular hops have $J_{i,j} > \text{cut-off}$, thereby, allowing clusters to form between molecules.

**Figure S5.** Visualizations of the clusters in the a) amorphous, b) semi-crystalline, and c) crystalline systems with size > 6 monomer units, given the following clustering criteria: transfer integral > 0.2 eV.

49 Now, we compare the clusters identified with the $J_{i,j}$ cut-off between the three systems. The
 50 crystalline morphology shows one large cluster (shown in red) and a few smaller clusters with opposing

Table S3. Table of cluster statistics for the three systems, given the following clustering criterion: transfer integral $J_{i,j} > 0.2$ eV.

Property	Amorphous	Semi-Crystalline	Crystalline
Mobility (cm^2/Vs)	1.02×10^{-1}	1.63×10^{-2}	1.16×10^{-1}
$J_{i,j}$ cut-off (eV)	0.200	0.200	0.200
Total clusters (Arb. U.)	289	163	64
Large (> 6) clusters (Arb. U.)	273	151	51
Largest cluster size (Arb. U.)	2564	9914	12837

51 grain orientations, indicating that the crystalline system will have a high connectivity. Conversely,
 52 the amorphous morphology is predicted to have poor connectivity based on this clustering metric
 53 stemming from the larger number of small clusters. However, the connectivity in the semi-crystalline
 54 morphology again shows a cluster arrangement intermediate between the other two. This cluster
 55 arrangement would again predict a high mobility for the crystalline morphology, a low mobility for
 56 the amorphous morphology and an intermediate morphology in the semi-crystalline case, which is
 57 contrary to our mobility calculations. Varying the cut-off to any consistent value between the three
 58 morphologies always results in this conclusion, suggesting that the transfer integral distribution is not
 59 an adequate way to identify clusters in the morphology.

60 3. Clustering Based on Hops

61 One short-coming of the previous clustering algorithms is that it considers charge transport
 62 between two chromophores in isolation. However, in the KMC algorithm, hops to all neighboring
 63 chromophores are considered and the preferential hop (based on the hopping rate between i and j
 64 and the random number x) will be chosen. As such, a “good” hop may not occur because there is a better
 65 hop.

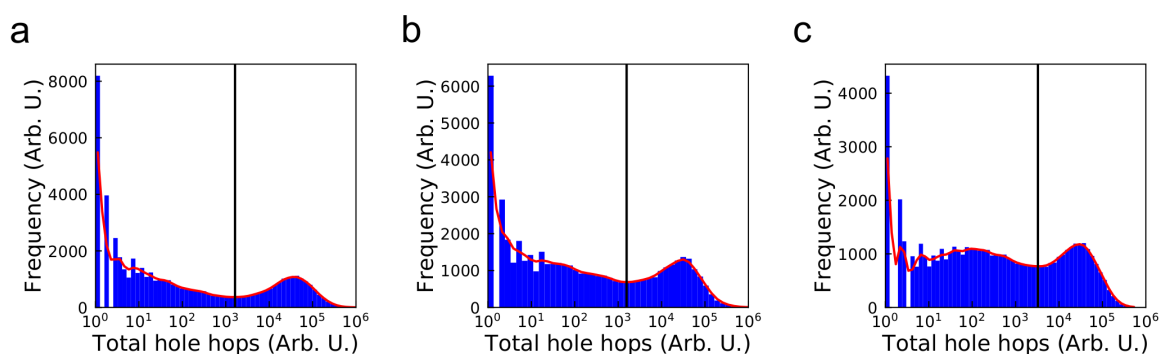


Figure S6. Distributions of the frequencies with which carriers hop between chromophore Voronoi neighbors for the representative 1,000 molecule a) amorphous, b) semi-crystalline, and c) crystalline morphologies. The red line shows the Gaussian filtered distribution shape that was used to determine the cluster cut-off criterion. The black vertical line shows the value of the cut-off criterion, which was automatically determined to be at the final minimum of the frequency distribution: a total of 3264, 1566, and 1635 hops for the crystalline, semi-crystalline, and amorphous systems respectively.

66 As such, defining clusters based on regions in which charges will freely move is prudent, however,
 67 we must still identify a sensible cut-off in hopping frequency to separate these regions. The distributions
 68 of total hole hops between chromophore pairs in the three representative systems are shown in
 69 [Figure S6](#). Note that the x-axis in these plots is logarithmic, leading to quantization of the bins on
 70 the left-hand side of the plot. In all three systems, a second peak appears at high hop frequencies.
 71 This leads to a local minimum at 3264 hops in the crystalline case, 1566 hops in the semi-crystalline

72 case, and 1635 hops in the amorphous case. We therefore use these values as the clustering criteria
 73 - only chromophores with connections that are used more than this number during the simulation
 74 will be added to the same cluster. We note that the exact values of the cut-off criteria are strongly
 75 dependent on the duration of the KMC simulation; the value may change significantly if fewer carriers
 76 iterations are performed or if simulation times are reduced. In this study, all three systems used the
 77 same simulation time-scales for KMC and the same number of carriers were averaged over in order to
 78 obtain the charge transport properties.

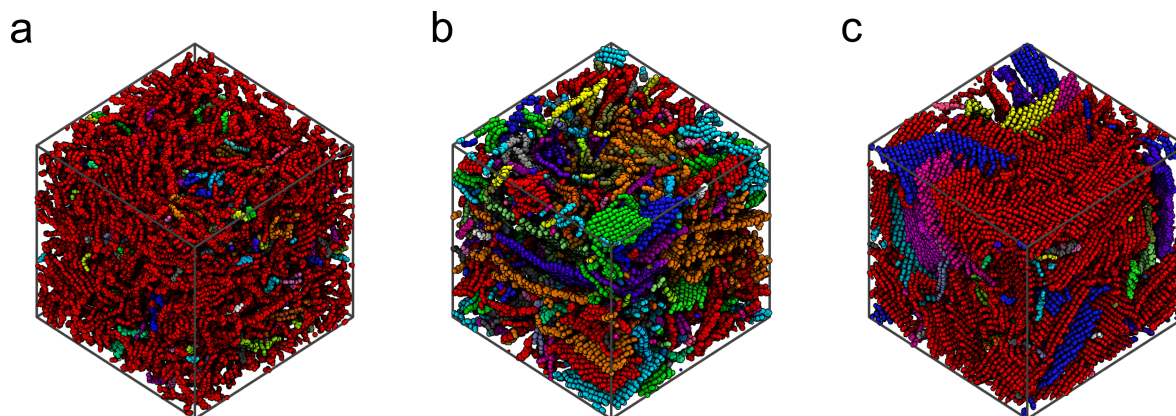


Figure S7. Visualizations of the clusters in the a) amorphous, b) semi-crystalline, and c) crystalline systems with size > 6 monomer units. Clusters were determined based on an automatically-defined hopping frequency cut-off for each system based on the distributions in [Figure S6](#).

Table S4. Table of cluster statistics for the three systems, given the automatically-defined total hop frequency cut-off criteria.

Property	Amorphous	Semi-Crystalline	Crystalline
Mobility (cm ² /Vs)	1.02×10^{-1}	1.63×10^{-2}	1.16×10^{-1}
Hop frequency cut-off (s ⁻¹)	1635	1566	3264
Total clusters (Arb. U.)	410	1376	418
Large (> 6) clusters (Arb. U.)	134	209	73
Largest cluster size (Arb. U.)	11867	3164	10254

79 The cluster visualizations using the hop frequency cut-off are shown in [Figure S7](#) are very
 80 promising. The crystalline morphology shows different crystalline grains very clearly - although the
 81 majority of the simulation is a single cluster (red), a large cluster with a different grain orientation
 82 is clearly visible in the morphology (blue). It is harder to distinguish the cluster distributions of the
 83 semi-crystalline and amorphous systems using the visualizations, although the crystals present in the
 84 semi-crystalline morphology are clearly resolvable from the amorphous matrix surrounding them.
 85 However, [Table S4](#) shows the first set of cluster properties where the semi-crystalline morphology
 86 is not intermediate between the crystalline and amorphous system, in terms of the number of total
 87 clusters and the largest cluster size. These clusters describe regions of the morphology that carriers
 88 are frequently hopping within. With this definition, hops within the regions are more common than
 89 those between clusters and so carriers are effectively trapped in this region - time is still progressing as
 90 they hop around, but their mean squared displacement is not significantly increasing. Therefore, a
 91 small number of large clusters is advantageous, whereas a large number of small clusters will strongly
 92 restrict charge transport properties.

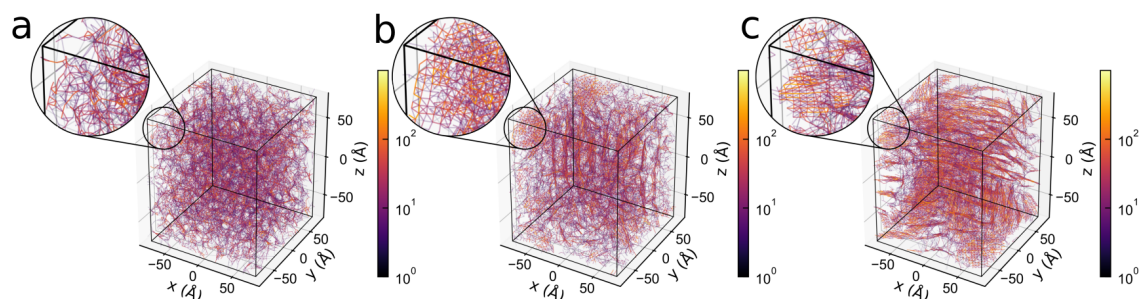


Figure S8. The network diagrams for the (a) amorphous, (b) semi-crystalline, and (c) crystalline systems show carrier pathways between connected chromophores (insets: zoomed regions). Connections are colored based on a perceptually uniform, logarithmic heatmap, where brighter zones correspond to more frequently used pathways.

93 4. Intra-cluster trapping

94 In our investigation, we record the location history of every carrier as it hops through the system.
 95 Using the carrier hopping history, we can construct network connectivity diagrams (Figure S8) to
 96 observe the most frequently travelled paths for charges through the morphology. These network
 97 connectivity diagrams are constructed by identifying the frequency with which holes in the KMC
 98 simulation hop between pairs of chromophores. The centre-of-mass locations of the chromophores
 99 then form the nodes of the network, and the shortest paths between each of the chromophore pairs
 100 become the edges. The “net hopping frequency” is calculated by subtracting the frequency of forward
 101 hops from backward hops and taking the absolute value. These values are normalized to the highest
 102 net hopping frequency in the system, and then assigned a color based on the logarithmic color map to
 103 highlight preferred carrier transport routes through the morphology.

104 The differences in structure between the three classes of morphology are clearly evident in
 105 Figure S8. The amorphous network graph (Figure S8a) shows that no crystallites have formed in the
 106 system. There are several high-traffic nodes spread homogeneously throughout the system, explaining
 107 the highly isotropic carrier trajectory presented in the main text. The crystalline network graph
 108 (Figure S8c) shows the lamellar structure of the system, with nearly all chains aligned in layers moving
 109 left-to-right across the morphology. The most frequently used pathways are along chains, and there are
 110 many connections in the π -stacking direction between chains within the crystal. The semi-crystalline
 111 network graph (Figure S8b) exhibits behaviour intermediate between the other two - crystallites with
 112 varying grain orientations are clearly visible, within an amorphous matrix.

113 The insets in Figure S8 show a zoomed region in the corner of the morphology, to highlight an
 114 area of ‘cross-hatching’ in the network, where carriers frequently loop around the same subset of
 115 chromophores (located at the vertices of the patterns), without increasing mean squared displacement
 116 (MSD) from their initial position. In the amorphous morphology (Figure S8a), no loops are observed,
 117 and therefore every hop (no matter how slow) is contributing to the MSD, increasing mobility. In
 118 the semi-crystalline (Figure S8b) and crystalline (Figure S8c) systems, significant looping can be seen.
 119 Carriers in these regions are becoming ‘trapped’ by the loops - even though transport may be fast
 120 between the chromophores, it becomes more difficult for the carriers to leave the crystal along the slow
 121 transport routes due to the wealth of fast hops available within. For the crystalline case, the morphology
 122 is dominated by one large crystallite that extends across the full simulation volume. Therefore, carriers
 123 getting trapped inside this crystallite are still able to move long distances, and the penalty to the
 124 mobility from the trapping is lessened (reflected by a high mobility and a larger anisotropy in the main
 125 text). However, in the semi-crystalline case, the morphology is composed of multiple crystallites with
 126 various orientations, with loops present across all three dimensions. Trapping therefore has a more
 127 significant effect - carriers get stuck in the small loops and are unable to increase their mean squared
 128 displacement over time in a single direction, restricting the carrier mobility within the system. These

129 conclusions are supported by the cluster maps presented in Figure S8, as well as the cluster properties
 130 presented in Table 1; the crystalline and amorphous systems are dominated by a single, well-connected
 131 cluster of chromophores permitting a high mobility, whereas the semi-crystalline system is composed
 132 of many clusters with differing grain orientations. The visualizations of the network in Figure S8 serve
 133 to provide additional evidence as to why the clusters described in the main text form within these
 134 morphologies.

135 5. Polydisperse Simulations

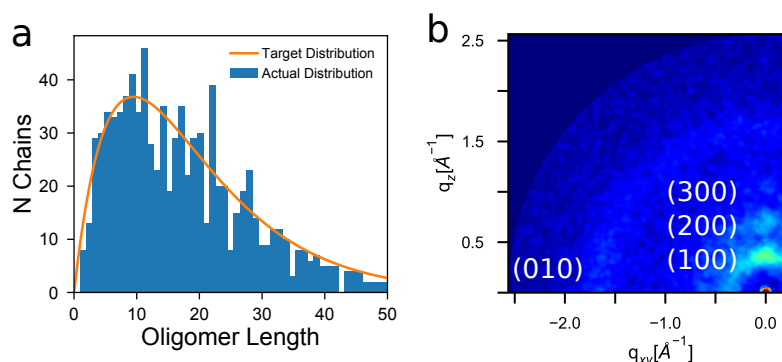


Figure S9. (a) The scaled target distribution of chain lengths and the histogram of the actual chain lengths used in the polydisperse simulations. (b) The equilibrated polydisperse systems is able to produce periodic features not seen in systems where all the chains are longer.

136 Here we present how we generate polydisperse P3HT simulations. This can be broken into two
 137 steps: first creating a dictionary of P3HT oligomers of varying lengths from 1 to 50 monomers long.
 138 Second is using a distribution to determine the amount of each chain length to place into the simulation.
 139 To produce chains of arbitrary length, we use the open-source program mBuild in which a polymer
 140 can be easily created using monomer building blocks. We limit the chain length used in this study at
 141 50 monomers long as to avoid unphysical interactions of chains feeling themselves across periodic
 142 boundaries. To generate the distribution of chain-lengths, we use the Schulz-Flory distribution which
 143 is a commonly used mathematical description for polymer lengths in the form [3]:

$$P_L = \alpha^2 D_P ((1 - \alpha)^{D_P - 1}), \quad (1)$$

144 in which P_L is the probability of seeing a chain of a given length, D_P is the degree of polymerization of
 145 a particular chain, and α is a tunable parameter which affects the shape of the distribution. The value
 146 for α used in this study was 0.1 and was chosen as this value produces polydispersities of ~ 1.8 .

147 To create the actual distribution of chain lengths we utilize a simple Monte Carlo algorithm. In
 148 this algorithm we select a random chain length between 1 and 50 and a random number (x) associated
 149 with this chain length between 0 and 1. If x is less than the probability of seeing a chain of that length
 150 $P(L)$ we accept the chain otherwise the chain is rejected. In addition to this, to ensure that we have the
 151 same number of monomers as the other simulations (15,000 monomers) we keep track of the number
 152 of monomers which have been added to the simulation. When the number of monomers added to
 153 the simulation via the Monte Carlo algorithm is less than 50 monomers from 15,000 monomers, we
 154 terminate the Monte Carlo algorithm and add the remaining monomers to the simulation via one more
 155 single chain so that the total number of monomers is 15,000 monomers.

156 After the Monte Carlo algorithm is finished and a distribution of the chain lengths suggested, we
 157 calculate the polydispersity of the simulation with:

$$PDI = \frac{M_w}{M_n}, \quad (2)$$

158 in which M_w is the weight average molecule weight and M_n is the number average molecule weight.
 159 M_w and M_n can be calculated with:

$$M_w = \frac{\sum N_i M_i^2}{\sum N_i M_i} \quad (3)$$

$$M_n = \frac{\sum N_i M_i}{\sum N_i}, \quad (4)$$

160 in which N_i is the number of chains of that length and M_i is the molecular weight of that chain
 161 length. If the PDI of the stochastically generated distribution of chain lengths is below 1.8, we reject
 162 the distribution and regenerate the distribution until $PDI \geq 1.8$. A comparison between the target
 163 distribution and the histogram of chain lengths is shown in [Figure S9a](#).

164 The distribution of chains presented in [Figure S9a](#) is able to produce ordered morphologies with
 165 periodic features ([Figure S9b](#)) along (100) and (010) signifying π - and alkyl-stacking. These features
 166 are seen in experimental and 15mer scattering patterns [4]. However, when simulating systems
 167 that contain only 50 membered chains, the system requires much longer to relax into these periodic
 168 structures.

169 **Acknowledgments:** This work used the Extreme Science and Engineering Discovery Environment (XSEDE),
 170 which is supported by National Science Foundation grant number ACI-1053575 [5]. This material is based upon
 171 work supported by the National Science Foundation under Grant No. (1229709) and (1653954), and (1658076).
 172 The authors thank Chris Muhich for his assistance in comparing ZINDO/S to DFT.

173 **Author Contributions:** Funding acquisition, Eric Jankowski; Investigation, Evan Miller and Matthew Jones;
 174 Software, Evan Miller and Matthew Jones; Supervision, Eric Jankowski; Writing – original draft, Evan Miller,
 175 Matthew Jones and Eric Jankowski; Writing – review & editing, Evan Miller, Matthew Jones and Eric Jankowski.

176 **Conflicts of Interest:** The authors declare no conflict of interest.

177 Abbreviations

178	15mer - P3HT chain containing 15 monomers
179	50mer - P3HT chain containing 50 monomers
180	ϵ_s - solvent quality
181	KMC - Kinetic Monte Carlo
182	MD - Molecular Dynamics
183	μ_0 - Zero-field Mobility
184	OPLS - Optimized Performance for Liquid Simulations
185	OPV - Organic Photovoltaic
186	P3HT - Poly(3-hexylthiophene)
187	ψ - order parameter
188	ψ' - modified order parameter
189	ρ - density
190	σ - standard deviation
191	T - Temperature
192	VRH - Variable Range Hopping
193	QCC - Quantum Chemical Calculations
194	

195

- 196 1. Becke, A.D. Density-functional thermochemistry. III. The role of exact exchange. *The Journal of Chemical*
 197 *Physics* **1993**, *98*, 5648–5652, [[z0024](#)]. doi:10.1063/1.464913.

- 198 2. Krishnan, R.; Binkley, J.S.; Seeger, R.; Pople, J.A. Self-consistent molecular orbital methods. XX. A basis set
199 for correlated wave functions. *The Journal of Chemical Physics* **1980**, *72*, 650–654, [[arXiv:10.1063/1.438955](https://arxiv.org/abs/10.1063/1.438955)].
200 doi:10.1063/1.438955.
- 201 3. Flory, P.J. Random Reorganization of Molecular Weight Distribution in Linear Condensation Polymers.
202 *Journal of the American Chemical Society* **1942**, *64*, 2205–2212. doi:10.1021/ja01261a049.
- 203 4. Miller, E.; Jones, M.; Henry, M.; Chery, P.; Miller, K.; Jankowski, E. Optimization and Validation of Efficient
204 Models for Predicting Polythiophene Self-Assembly. *Polymers* **2018**, *10*, 1305. doi:10.3390/polym10121305.
- 205 5. Towns, J.; Cockerill, T.; Dahan, M.; Foster, I.; Gaither, K.; Grimshaw, A.; Hazlewood, V.; Lathrop, S.; Lifka,
206 D.; Peterson, G.D.; Roskies, R.; Scott, J.R.; Wilkens-Diehr, N. XSEDE: Accelerating Scientific Discovery.
207 *Computing in Science & Engineering* **2014**, *16*, 62–74. doi:10.1109/MCSE.2014.80.